

Spatial Throughput of Wireless Networks under Different Decoding Rules

Pedro H. J. Nardelli, *Student Member, IEEE*, Paulo Cardieri, *Member, IEEE*
and Matti Latva-aho, *Senior Member, IEEE*

Abstract

This paper revisits the problem of characterizing the highest spatial throughput – or spatial capacity – of wireless networks in $[\text{bits/s/Hz/m}^2]$ in light of some recent results. We analyze the expected maximum achievable sum rates over a given area based on the capacity regions of Gaussian point-to-point codes in Poisson distributed wireless networks under two decoding rules, namely (i) IAN: treating interference as noise, and (ii) OPT: jointly detecting the strongest interfering signals, treating the others as noise. We prove that the average spatial capacity is the product of the network density and the expected value of the achievable coding rates that maximize the spatial throughput for different network realizations. Assuming that the closest interferer power approximates the aggregate interference caused by all transmitters that are treated as noise, we analytically derive several properties of the average spatial capacity and evince the better performance of OPT decoders. We also compare these results to the ones obtained for a scenario where transmitters code their messages at predetermined fixed rates that are tuned to optimize the average spatial throughput, regardless of particular realizations of the network. Using this approach, however, some rates may not be achievable, yielding outage events. We analytically show that, when the same decoding rule and network density are considered, the spatial-capacity-achieving scheme always outperforms the spatial throughput obtained with the best predetermined fixed rate strategy. We then discuss the validity of our approximation using simulation results and implementation issues related to different mobility patterns.

Index Terms

Ad hoc networks, decoding rules, interference, network information theory, Poisson point process, spatial throughput, stochastic geometry

This work was supported in part by Infotech Graduate School, Finnish Funding Agency for Technology, and Innovation (Tekes), Nokia Siemens Networks, Elektrobit and CNPq-Brazil (Proc. No. 309597/2009-9).

Part of this work was presented in 2012 IEEE Wireless Communications and Networking Conference, Paris, Apr. 2012.

Pedro H. J. Nardelli is with Center for Wireless Communications (CWC), University of Oulu, Finland, and Wireless Technology Laboratory (WissTek), State University of Campinas, Brazil (e-mail: nardelli@ee.oulu.fi). Paulo Cardieri is with the WissTek. Matti Latva-aho is with CWC.

I. INTRODUCTION

In the last few years, the demands for more efficient, reliable wireless systems induced network designers to think about alternative ways to supplement centralized cellular models. One interesting idea is to build a multi-layer network where macro-base-stations coexist with a great number of smaller cells, which in turn operate in a more distributed fashion (e.g. the concept of femto-cell networks [1]). But differently from the centralized approach whose capacity are fairly well characterized by Shannon theory, the limits of distributed systems that work in interference-limited regimes are unknown except for few specific cases, as discussed in [2].

In 1978 Carleial formally stated the interference channel problem using arguments from information theory [3]. Since then, several results and bounds have been proposed for the interference channel as discussed in [4, Ch. 6]. Although these works put some light on the problem, the capacity region of the simplest two-source-two-destination setting is still an open problem. Moreover, when multiples sources and destinations are considered, such capacity regions becomes even more elusive.

Knowing such difficulties, some researchers have started investigating alternative approaches to better understand the limits of wireless networks with multiple communication pairs. Gupta and Kumar introduced in [5] the *transport capacity* metric to determine how many bits-meter a wireless network with uniformly distributed nodes can reliably sustain when its density grows to infinite (asymptotic analysis). After this milestone, many other papers have focused on a similar idea, finding the transport capacity scaling laws for different scenarios and under different assumptions. The monograph [6] compiles some of such studies.

Franceschetti et al. presented another important result in [7], where they applied an unconventional method to find the physical limit of wireless networks by using laws of electrodynamics. The authors further extended this approach in a recent work [8] and determined the degrees of freedom of wireless networks based on electromagnetic theory.

Nevertheless both Franceschetti's and Gupta's lines of research strongly rely on the asymptotic behavior of the network with the number of nodes infinitely growing, which may give an unclear picture of the physical or medium access control network layers' design. Bearing this aspect in mind, Weber et al. applied in [9] a statistical approach to characterize the throughput of wireless networks and then defined the *transmission capacity* as the highest *spatial throughput*¹ achievable without exceeding a maximum link outage probability, using the density of active links as the optimization variable. An important aspect of this

¹In the literature, spatial throughput can be also referred to as *area spectral efficiency* [10].

work is the use of stochastic geometry [11] to characterize the node spatial distribution as a Poisson point process (PPP). Thereafter different strategies used in the wireless communications have been investigated such as interference cancellation, threshold transmissions, guard zones, bandwidth partitioning amongst others; the reference [12] compiles these results.

In addition to them, we find in the literature other contributions using a similar approach. For example, Vaze studied in [13] the throughput-delay-reliability trade-off in multi-hop networks using the metric *random access transport capacity*, which is an extension of the transmission capacity for multi-hop systems [12, Sec. 4.2]. In [14] the authors assessed how the hopping strategy affect the *aggregate multi-hop information efficiency* of ad hoc networks, while in [15] they studied a revisited version of the transmission capacity to compare different modulation-coding schemes. The work [16] presents the transmission capacity optimization in term of the number of allowed retransmissions considering different MAC protocols. Ganti et al. generalized in [17] the transmission capacity for different fading and node distributions for the high SIR regime.

Apart from these recent papers that focus on the statistic quantification of the spatial throughput of wireless networks, the use of models from stochastic geometry dates back the early 80's, when Takagi and Kleinrock firstly introduced the idea of evaluating the aggregate interference power of Poisson distributed interfering nodes [18]. Thereafter, the subject has greatly developed and we can cite [19]–[22] as relevant tutorials on how to apply stochastic geometry when analyzing wireless systems.

This paper aims at characterizing the spatial throughput of wireless networks specifically when transmitter nodes are spatially distributed following a PPP. To reach this goal, we review the results due to Baccelli et al. [23], where the authors studied the capacity regions of Gaussian point-to-point codes for interference networks. More specifically, we apply two different decoding rules described therein: *treating interference as noise* – the IAN rule – and *joint detection of the strongest interferers' messages and treating the others as noise*² – the OPT rule. Then, we use theorems from point process theory to obtain approximations and bounds of the highest achievable spatial throughput for a given network density, naming this maximum value as *spatial capacity*.

For comparison purposes, we also evaluate the highest spatial throughputs achieved when all links use fixed (symmetric) coding rates (which is the most usual approach as in [12], [23, Sec. IV], [24]). We then proceed with an unconstrained optimization of the *average* spatial throughput over different

²This rule splits the set of interferers into two mutually exclusive subsets: one contains the strongest interferers whose messages will be joint decoded with the desired one, and the other contains the transmitters with weaker detected power that will be treated as noise. This strategy is proved in [23] the optimal for Gaussian point-to-point codes over interference channels, as discussed later on.

spatial realizations, where the optimization variable is the rate that the transmitters code their messages. Differently from the spatial-capacity-achieving scenario where the coding rates are tuned to be the highest achievable rates given the relative nodes' positions for each different spatial realization, the fixed rate scheme only cares about the average behavior of the network, resulting in decoding errors (outage events) for links whose capacity is below that predetermined rate. We analytically prove that, under the same assumptions, such a strategy performs worse than the spatial-capacity-achieving one. Our numerical results illustrate this difference as well as the advantages of using OPT instead of IAN³.

We also simulate the network to validate our findings, justifying why our analysis is relevant even when our approximations are loose. Besides we discuss the feasibility of the decoding rules and optimization strategies for different mobility patterns: for (quasi-)static topologies, the spatial capacity can be achieved; for highly mobile topologies, it cannot and the fixed rate optimization with IAN turns out to be the most appropriate choice. From this perspective, we list the reasons to use cognitive, adaptive algorithms to improve the performance of wireless networks when mobility patterns are unknown.

The rest of this paper is divided as follows. In Section II, we first revisit the capacity region of Gaussian point-to-point codes over interference channels [23] and then define the spatial capacity of wireless networks. Section III presents the network modeling together with some general results for Poisson networks. Section IV analyzes the IAN decoder, while the OPT is the focus of Section V. A comparison between the spatial-capacity-achieving and the symmetric rate scenarios is found in Section VI. We discuss the tightness of our approximations and implementation issues in Section VII, followed by the final remarks in Section VIII.

II. CAPACITY REGION OF GAUSSIAN POINT-TO-POINT CODES AND SPATIAL CAPACITY

This section reviews the capacity region of Gaussian point-to-point (G-ptp) codes for an arbitrary number of communication pairs, which was firstly stated by Baccelli et al. in [23, Sec. II] and is also fundamental for the study carried out here.

Let us assume a network with area A [m²] where $K+1$ source-destination pairs (also called transmitter-receiver pairs) coexist. Each source node $i \in [0, K]$ wants to transmit an independent message $M_i \in [1, 2^{nR_i}]$ to its respective destination i at rate R_i [bits/s/Hz], where n is the codeword length. Let X_j be the complex signal transmitted by source $j \in [0, K]$ and let $Z_i \sim \mathcal{CN}(0, 1)$ be the complex circularly

³We do not assume any *interference cancellation* (IC) technique as in [12, Sec. 4.2], [25]–[27] since the OPT rule used in this paper always performs better than IC, as discussed in [23], [24]. In addition, we consider no kind of strong coordination between the active links so that the *interference alignment* method [28] is unfeasible; a detailed discussion about it can be found in [23, Sec. III].

symmetric Gaussian random variable that represents the noise effect at receiver i . The detected signal Y_i at receiver i is then:

$$Y_i = \sum_{j=0}^K g_{ij} X_j + Z_i, \quad (1)$$

where g_{ij} are the complex channel gains between transmitter j (TX $_j$) and receiver i (RX $_i$). We assume that every transmitted signal is subject to the same power constrain of Q [W/Hz] so the received signal between TX $_j$ and RX $_i$ is constrained by $P_{ij} = |g_{ij}|^2 Q$.

Each transmitter node uses a G-ptp code with a set of randomly and independently generated codewords $x_i^n(m_i) = (x_{i1}, \dots, x_{in})(m_i)$ following i.i.d. $\mathcal{CN}(0, \sigma^2)$ sequences such that $0 < \sigma^2 \leq Q$, where $m_i \in [1, 2^{nR_i}]$, $i \in [0, K]$. RX $_i$ receives a signal y_i^n over the interference channel given by (1) and then estimates the transmitted message as $\hat{m}_i(y_i^n) \in [1, 2^{nR_i}]$. An error event in the decoding happens whenever the transmitted message differs from the estimated one. Therefore the error probability of the G-ptp code is:

$$p_n = \frac{1}{1+K} \sum_{i=0}^K \Pr[\hat{M}_i \neq M_i]. \quad (2)$$

Next we use (2) to define the achievable rates and the capacity region for G-ptp codes.

Definition 1 (achievable rates and capacity region): Let \bar{p}_n be the average of the error probability p_n over G-ptp codes where n is the codeword length. Then, a rate tuple $\mathbf{R} = (R_0, \dots, R_K)$ is said to be achievable if $\bar{p}_n \rightarrow 0$ when $n \rightarrow \infty$. In addition, the capacity region using G-ptp codes is the closure of the set of achievable tuple rates \mathbf{R} .

This definition is important in our context because the spatial-capacity-achieving setting always requires achievable rates, as we will discuss later. But before that, we apply Definition 1 to establish the the capacity region of G-ptp codes.

Theorem 1 (capacity region from [23]): Let \mathcal{A} be the set of all $K+1$ transmitters in the network. Let \mathcal{A}_i denote a subset of \mathcal{A} that contains TX $_i$ with $i \in [0, K]$ and $\bar{\mathcal{A}}_i$ its complement. RX $_i$ then observes a multiple access channel (MAC) whose capacity region \mathcal{R}_i is computed as

$$\mathcal{R}_i = \left\{ \mathbf{R} : \sum_{k \in \mathcal{A}_i} R_k \leq \log_2 \left(1 + \frac{\sum_{k \in \mathcal{A}_i} P_{ik}}{1 + \sum_{j \in \bar{\mathcal{A}}_i} P_{ij}} \right) \forall \mathcal{A}_i \subseteq \mathcal{A} \right\}. \quad (3)$$

The capacity region \mathcal{R} of the Gaussian interference channel with G-ptp codes is the intersection of the

capacity regions \mathcal{R}_i of all TX_{*i*}-RX_{*i*} links with $i \in [0, K]$, i.e.

$$\mathcal{R} = \bigcap_{i=0}^K \mathcal{R}_i. \quad (4)$$

Proof: The proof of this theorem is found in [23, Sec. II]. ■

The capacity region stated above requires a decoder that treats some of the interferers as noise, while others have their messages jointly decoded with the desired one. This result is the basis of the OPT strategy mentioned in the previous section and further studied in Section V.

Now we define the network spatial throughput and then use Theorem 1 to define the spatial capacity as the highest achievable spatial throughput.

Definition 2 (spatial throughput): Let $A [m^2]$ be the network area. Then the spatial throughput, denoted by \mathcal{S} and measured in $[bits/s/Hz/m^2]$, is defined as

$$\mathcal{S} = \frac{1}{A} \sum_{i=0}^K R_i. \quad (5)$$

Definition 3 (spatial capacity of a given spatial realization): The spatial capacity, denoted by \mathcal{S}^* , is defined as the maximum spatial throughput of the network such the rate tuple is achievable – $\mathbf{R} = (R_0, \dots, R_K) \in \mathcal{R}$. Then,

$$\mathcal{S}^* = \max_{\mathbf{R} \in \mathcal{R}} \mathcal{S}. \quad (6)$$

The spatial capacity reflects the highest sum of achievable rates over a given area and it may have a huge variation depending on the network topology (i.e. the number and/or position of the transmitter–receiver pairs). To deal with this issue, we opt for studying Poisson distributed networks that are analytically tractable, allowing us to derive approximate expressions for the expected spatial capacity \mathcal{S}^* (over different spatial realizations).

III. SPATIAL CAPACITY OF POISSON NETWORKS

Let Φ be a two-dimensional homogeneous Poisson point process (PPP) with density λ [nodes/m²] that characterizes the spatial distribution of transmitters (TXs) over \mathbb{R}^2 . We assume that each TX is associated with one receiver (RX) located at a fixed distance d from it in a random orientation⁴ to establish a communication link; this is also known as *Poisson bipolar model* [19]. In addition, we consider that all TXs transmit information to their intended RXs over the same frequency band with width of W [Hz] (narrow-band) and using the G-tp codes described in Section II.

⁴Note that the RXs are not part of the process Φ .

For each realization of Φ , the network may have a different capacity region \mathcal{R} and consequently a different spatial capacity \mathcal{S}^* . Even worse, when the network area is the infinite plane (i.e. \mathbb{R}^2), the capacity region given by equation (4) becomes impossible to be computed. Knowing these limitations, we define the average spatial capacity as the expected value of the highest achievable spatial throughputs, which allows us to analyze the performance of infinite networks over different spatial realizations of Φ .

Definition 4 (average spatial capacity): Let $\mathbf{R} = (R_0, \dots, R_K)$ be a tuple rate and \mathcal{R} be the capacity region for a given network realization, then the average spatial capacity \mathcal{C} is defined as

$$\mathcal{C} = \mathbb{E}[\mathcal{S}^*] = \mathbb{E} \left[\max_{\mathbf{R} \in \mathcal{R}} \frac{1}{A} \sum_{i=0}^K R_i \right], \quad (7)$$

where $\mathbb{E}[\cdot]$ represents the expected value.

We can now apply properties from the point process theory to compute the spatial capacity of this class of Poisson networks as follows.

Lemma 1 (average spatial capacity): The average spatial capacity \mathcal{C} is computed for the Poisson network described in this section as

$$\mathcal{C} = \lambda \mathbb{E}[R^*], \quad (8)$$

where λ is the network density and R^* is the random variable that characterizes the spatial-capacity achievable rates over the infinite plane and network realizations.

Proof: Let us first remind that the spatial process Φ takes place in \mathbb{R}^2 and then $A \rightarrow \infty$, $K \rightarrow \infty$ and $\mathbf{R} = (R_0, R_1, \dots)$. Then, we proceed with the following manipulation:

$$\mathcal{C} = \mathbb{E} \left[\max_{\mathbf{R} \in \mathcal{R}} \lim_{A \rightarrow \infty} \frac{1}{A} \sum_{i=0}^{\infty} R_i \right], \quad (9)$$

$$\stackrel{(a)}{=} \mathbb{E} \left[\lim_{A \rightarrow \infty} \frac{1}{A} \sum_{i=0}^{\infty} R_i^* \right], \quad (10)$$

$$\stackrel{(b)}{=} \lambda \mathbb{E}[R^*]. \quad (11)$$

Specifically, equality (a) considers the value of $\mathbf{R}^* = (R_0^*, R_1^*, \dots) \in \mathcal{R}$ that leads to the maximum spatial throughput for a given network realization, resulting in the spatial capacity \mathcal{S}^* . Equality (b) comes from a straight application of Campbell theorem [11, Th. 2.2] in equation (7), considering that Φ has spatial intensity of λ [TXs/m²]. The rates R_i^* 's that guarantee a successful communication are determined by random variables that depend on the network topology for each realization of Φ . As homogeneous PPPs are stationary and isotropic, we can apply the concept of Palm distribution and Slivnyak theorem

[11, Ch. 3] to determine the statistical proprieties of any node in Φ based on a typical node. Then, we can determine the expected value of the spatial-capacity achievable rates over \mathbb{R}^2 and over different realizations of Φ based on such a node and hence the index i can be dropped, which concludes this proof. ■

Remark: We can generalize this results for different stationary and isotropic point processes. It is also possible to use a similar approach to compute the spatial capacity of more general processes using the Campbell theorem and Palm distributions accordingly.

From equation (8), one can see that the main problem is now to derive the distribution of the spatial-capacity achievable rates R^* , which is our focus in the next two sections.

IV. INTERFERENCE AS NOISE DECODING RULE

In this section we assess the decoding rule where the receivers treat the interference as noise – or IAN decoders. The following corollary shows its achievable rates.

Corollary 1 (achievable rates for IAN decoders): Assuming the noise is Gaussian and considering that TXs employ G-ptp codes as described in Section II, the rate R_k associated with a given link $\text{TX}_k\text{-RX}_k$ is achievable when IAN decoders are used if, and only if, the following inequality holds:

$$R_k \leq \log_2 \left(1 + \frac{P_{kk}}{1 + \sum_{j \in \mathcal{A} \setminus \{k\}} P_{kj}} \right), \quad (12)$$

where \mathcal{A} represents the set of active transmitters.

Proof: This is a special case of (3) assuming that RX_k only decodes the message of TX_k while the other TXs are treated as noise. ■

We now apply this corollary to the scenario described in Section III to assess the spatial capacity of Poisson networks when receivers use IAN decoders. Before we start, however, we still need to characterize the propagation phenomenon. We consider here the distance-dependent path-loss modeling with exponent $\alpha > 2$ [29] so the channel gain between TX_j and RX_i is $|g_{ij}|^2 = x_{ij}^{-\alpha}$, where x_{ij} denotes the distance between them⁵. We assume the noise power is negligible in comparison to the interference power (interference-limited regime). We further consider that the aggregate interference experienced by RX_k can be approximated by power $P_{k,\text{clo}}$ related to its closest interferer. Mathematically we have the

⁵This is in fact a simplified model that may lead to meaningless results for $x_{ij} < 1$. As pointed in [30], modified versions of this model just increase the complexity of the analysis without providing significant differences. We can also include into our channel modeling the effects of random fluctuations due to shadowing and multi-path as in [12, Sec.4.1]. For our purposes, though, the incorporation of these phenomena only complicates the mathematical formulation without giving any further insight on the network behavior.

following⁶: $1 + \sum_{j \in \mathcal{A} \setminus \{k\}} P_{kj} \approx P_{k,\text{clo}}$.

Based on these assumptions, we can derive an approximation of the probability density function (pdf) of the spatial-capacity-achieving rates for IAN decoders as presented next.

Proposition 1 (approximate pdf of the spatial-capacity-achieving rates for IAN): Let $\mathbf{R}^* = (R_0^*, R_1^*, \dots) \in \mathcal{R}$ be the rate tuple that achieves the spatial capacity for the network described in Section III. The pdf of R_i^* , $\forall i \in \mathcal{A}$ over the different spatial realizations is equivalent to the pdf $f_{R^*}(x)$ of a typical rate R^* , which is approximated by

$$f_{R^*}(x) \approx \ln 4 \frac{2^x \lambda \pi d^2 (2^x - 1)^{\frac{2}{\alpha}}}{\alpha (2^x - 1)} e^{-\lambda \pi d^2 (2^x - 1)^{\frac{2}{\alpha}}}, \quad (13)$$

where $x > 0$.

Proof: Let us analyze a typical link $\text{TX}_0\text{--RX}_0$ added to the PPP Φ . From Slivnyak theorem (refer to [11, Th. 3.1]), this inclusion does not affect the distribution of Φ . Without loss of generality, we assume that the origin of the plane is located at RX_0 and label the interferers TX_i accordingly to their distances to RX_0 , i.e. TX_1 is the closest, TX_2 is the second closest and so on. From our assumptions, we have $1 + \sum_{k=1}^{\infty} P_k \approx P_1$. We then apply the path-loss model to the IAN decoder presented in equation (12), considering that the distances from TX_0 and TX_1 to RX_0 are respectively $d > 0$ and $r_1 > 0$, resulting in

$$R_0 \leq \log_2 \left(1 + \frac{d^{-\alpha}}{r_1^{-\alpha}} \right), \quad (14)$$

where r_1 is a random variable.

To compute the pdf of r_1 , we use the definition of contact zone [11, Defs. 1.9, 3.2] (the distance between a typical point and its first neighbor) to obtain the pdf of r_1 , resulting in [31]

$$f_{r_1}(x) = 2\lambda\pi x e^{-\lambda\pi x^2}, \quad (15)$$

such that $x > 0$. Defining $\beta_0^* = d^{-\alpha}/r_1^{-\alpha}$ such that inequality (14) still holds, then we have the following relation $r_1 = d\beta_0^{*\frac{1}{\alpha}}$ (see Fig. 1). We now apply this variable transformation to (15) and hence the pdf of $\beta_0^* > 0$ can be obtained as

$$f_{\beta_0^*}(x) = \frac{2\lambda\pi d^2 x^{\frac{2}{\alpha}}}{\alpha x} e^{-\lambda\pi d^2 x^{\frac{2}{\alpha}}}, \quad (16)$$

where $x > 0$.

⁶This approximation is analyzed in [25] and it usually applied to compute lower bounds of the interference power based on *dominant interferers* [12], [14]. We also discuss more about it in Section VII.

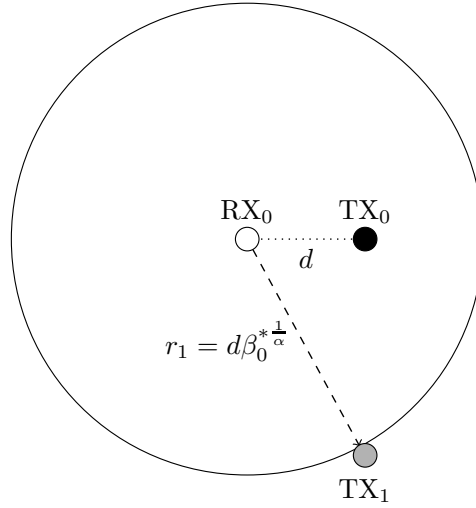


Fig. 1. Illustrative example of the typical link $\text{TX}_0\text{--RX}_0$ employing the IAN decoding rule, where TX_1 represents the closest interferer to RX_0 . To reach the highest achievable rate R_0^* , the relation $r_1 = d\beta_0^{*\frac{1}{\alpha}}$ must be respected such that r_1 is the random variable that denotes the distance between RX_0 and TX_1 .

To conclude this proof, we proceed with the transformation $R_0^* = \log_2(1 + \beta_0^*)$ remembering that PPPs are stationary so we can characterize any node of the network based on a typical node, dropping the index 0 (refer to [11, Sec. 3.4]). ■

The result just stated provides us an approximation⁷ of pdf of the spatial-capacity-achieving rates using IAN decoders over an infinite plane and over different spatial realizations of the process Φ . Then, we apply (13) to approximate the spatial capacity given by (8), resulting in

$$\mathcal{C}_{\text{IAN}} \approx \lambda \int_0^\infty x f_{R^*}(x) dx, \quad (17)$$

which does not have a closed-form solution and a numerical integration is required. For this reason, next we derive some proprieties⁸ of (17) that help us to understand the \mathcal{C}_{IAN} behavior.

Property 1 (concavity of the spatial capacity): A function $f(\cdot)$ is said to be *quasi concave* if, and only if, $f(px_1 + (1-p)x_2) \geq \min\{f(x_1), f(x_2)\}$, where $0 \leq p \leq 1$. Considering that the rate that leads to the spatial capacity, R^* , is a function of the network density λ (i.e. $R^* = f(\lambda)$), then \mathcal{C}_{IAN} given by (17) is *quasi concave* in terms of λ , where R^* is a random variable characterized by the pdf (13).

⁷We discuss the tightness of the closest interferer approximation later in Section VII.

⁸Such properties rely on the closest interferer approximation that will be discussed later on. For simplicity we hereafter refer to the approximate average spatial capacity as spatial capacity.

Proof: Let us first consider two different network densities λ_1 and λ_2 such that $\lambda_1 < \lambda_2$. Then, defining that $\lambda = p\lambda_1 + (1-p)\lambda_2$ with $0 \leq p \leq 1$, we proceed with the following manipulation

$$\mathcal{C}_{\text{IAN}}(\lambda) = (p\lambda_1 + (1-p)\lambda_2) \mathbb{E}[f(p\lambda_1 + (1-p)\lambda_2)] \quad (18)$$

$$\stackrel{(a)}{\geq} \lambda_1 \mathbb{E}[f(p\lambda_1 + (1-p)\lambda_2)] \quad (19)$$

$$\stackrel{(b)}{=} \lambda_1 \mathbb{E}[f(\lambda_1)] = \mathcal{C}_{\text{IAN}}(\lambda_1) \quad (20)$$

$$\stackrel{(c)}{\geq} \lambda_2 \mathbb{E}[f(\lambda_2)] = \mathcal{C}_{\text{IAN}}(\lambda_2). \quad (21)$$

Inequality (a) comes from the fact that $\lambda_1 \leq p\lambda_1 + (1-p)\lambda_2$ whereas equality (b) is obtained by setting $p = 1$ since the first inequality holds for all $0 \leq p \leq 1$. This proves the quasi concavity of the analyzed function when $\lambda_1 \mathbb{E}[f(\lambda_1)] < \lambda_2 \mathbb{E}[f(\lambda_2)]$. Finally, inequality (c) is straight when $\lambda_1 \mathbb{E}[f(\lambda_1)] \geq \lambda_2 \mathbb{E}[f(\lambda_2)]$, which concludes this proof. ■

Property 2 (highest spatial capacity): The network density λ^* that leads to the highest spatial capacity given by (17) is obtained as the density $\lambda > 0$ which is solution to the following equation:

$$\int_0^\infty x^{\frac{2}{\alpha}-1} \log_2(1+x) e^{-\lambda\pi d^2 x^{\frac{2}{\alpha}}} dx = \int_0^\infty x^{\frac{2}{\alpha}-1} \left(\lambda\pi d^2 x^{\frac{2}{\alpha}} - 1 \right) \log_2(1+x) e^{-\lambda\pi d^2 x^{\frac{2}{\alpha}}} dx. \quad (22)$$

Proof: Let us first rewrite the spatial capacity formulation using the pdf $f_{\beta^*}(x)$ given by (16), yielding

$$\mathcal{C}_{\text{IAN}} = \lambda \int_0^\infty \log_2(1+x) f_{\beta^*}(x) dx. \quad (23)$$

Then, we recall that the \mathcal{C}_{IAN} is quasi-concave in terms of λ (Property 1) to find its maximum value based on the derivative equation $d\mathcal{C}_{\text{IAN}}/d\lambda = 0$. After some algebraic manipulation, we obtain (22), which concludes this proof. ■

Property 3 (lower bound): A lower bound of the spatial capacity given by (17) is computed as

$$\mathcal{C}_{\text{IAN}} \geq \lambda y e^{-\lambda\pi d^2 (2^y - 1)^{\frac{2}{\alpha}}}, \quad (24)$$

where $y > 0$.

Proof: To prove this property, we apply the Markov inequality as presented below:

$$\Pr[R^* \geq y] \leq \frac{\mathbb{E}[R^*]}{y} \Rightarrow \mathbb{E}[R^*] \geq y e^{-\lambda\pi d^2 (2^y - 1)^{\frac{2}{\alpha}}}, \quad (25)$$

where $\Pr[R^* \geq y] = 1 - \int_0^y f_{R^*}(x) dx$ and $2^y - 1 > 0$.

Then, we multiply both sides by λ , resulting in (24). ■

Property 4 (upper bound): An upper bound of the spatial capacity given by (17) is computed as

$$\mathcal{C}_{\text{IAN}} \leq \lambda \log_2 \left(1 + \left(\frac{1}{\lambda \pi d^2} \right)^{\frac{\alpha}{2}} \Gamma \left(1 + \frac{\alpha}{2} \right) \right). \quad (26)$$

where $\Gamma(\cdot)$ is the Euler gamma function defined as $\Gamma(z) = \int_0^\infty t^{z-1} e^{-t} dt$.

Proof: Let us apply Jensen's inequality based on the concavity of (17) (refer to Property 1), yielding

$$\mathcal{C}_{\text{IAN}} = \lambda \mathbb{E}[R^*] \quad (27)$$

$$\stackrel{(a)}{=} \lambda \mathbb{E}[\log_2(1 + \beta^*)] \quad (28)$$

$$\stackrel{(b)}{\leq} \lambda \log_2(1 + \mathbb{E}[\beta^*]), \quad (29)$$

where equality (a) comes from the fact that $R^* = \log_2(1 + \beta^*)$ and inequality (b) is the Jensen inequality for quasi-concave functions. Then, we compute the expectation of the random variable β^* using (16), which proves (26). ■

Property 5 (asymptotic equivalence): Let \sim denote asymptotic equivalence of two functions, then

$$\mathcal{C}_{\text{IAN}} \sim c \lambda^{1-\frac{\alpha}{2}}, \quad (30)$$

when $\lambda \rightarrow \infty$ and $c = \left(\frac{1}{\pi d^2} \right)^{\frac{\alpha}{2}} \Gamma \left(1 + \frac{\alpha}{2} \right)$.

Proof: To prove that two functions $f(x)$ and $g(x)$ are asymptotically equivalent, i.e. $f(x) \sim g(x)$, we should show that $\lim_{x \rightarrow \infty} f(x)/g(x) = 1$. Let us first consider the behavior of the random variable β^* , characterized by (16) when $\lambda \rightarrow \infty$, yielding

$$\lim_{\lambda \rightarrow \infty} f_{\beta^*}(x) = \delta(x), \quad (31)$$

where $\delta(x)$ is the Dirac impulse function.

This indicates that the random variable β^* tends to have the value 0 with high probability when the network density increases. Now, let us consider that $\beta^* \rightarrow 0$, then we have the following limit

$$\lim_{\beta^* \rightarrow 0} \frac{\log_2(1 + \beta^*)}{\beta^*} = \frac{1}{\ln 2}. \quad (32)$$

Using these limits, we can manipulate the expression of the spatial capacity \mathcal{C}_{IAN} as follows.

$$\lim_{\lambda \rightarrow \infty} \mathcal{C}_{\text{IAN}} = \lim_{\lambda \rightarrow \infty} \lambda \mathbb{E}[\log_2(1 + \beta^*)] = \lim_{\lambda \rightarrow \infty} \lambda \frac{\mathbb{E}[\beta^*]}{\ln 2}. \quad (33)$$

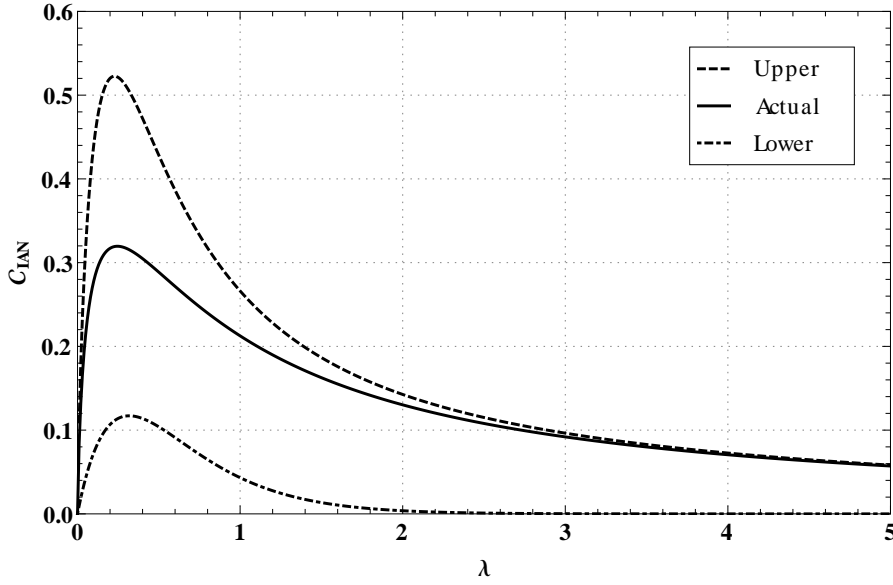


Fig. 2. Actual values, lower and upper bounds of the spatial capacity, C_{IAN} , versus the network density λ for $\alpha = 4$ and $d = 1$. The lower bound is obtained using $y = 1$ in equation (24). The actual values and upper bound are computed using equations (17) and (26), respectively.

Proceeding similarly with the upper bound, we have

$$\lim_{\lambda \rightarrow \infty} \lambda \log_2(1 + \mathbb{E}[\beta^*]) = \lim_{\lambda \rightarrow \infty} \lambda \frac{\mathbb{E}[\beta^*]}{\ln 2}. \quad (34)$$

Now, we recall that the division of limits is the limit of the division, resulting in

$$\lim_{\lambda \rightarrow \infty} \frac{\lambda \mathbb{E}[\log_2(1 + \beta^*)]}{\lambda \log_2(1 + \mathbb{E}[\beta^*])} = 1. \quad (35)$$

From this fact, we can state

$$C_{IAN} \sim \lambda \log_2 \left(1 + \left(\frac{1}{\lambda \pi d^2} \right)^{\frac{\alpha}{2}} \Gamma \left(1 + \frac{\alpha}{2} \right) \right), \quad (36)$$

when $\lambda \rightarrow \infty$.

To conclude this proof, we verify that $\left(\frac{1}{\lambda \pi d^2} \right)^{\frac{\alpha}{2}} \Gamma \left(1 + \frac{\alpha}{2} \right) \rightarrow 0$ when $\lambda \rightarrow \infty$ and then we apply the approximation $\log(1 + x) \approx x$ valid when $x \ll 1$ into (36) resulting (30). ■

Fig. 2 illustrates the behavior of the spatial capacity C_{IAN} and its proposed bounds as a function of the network density λ . Firstly, one can notice that the spatial capacity has a maximum point which is expected from its concavity stated in Property 1 and the density λ^* that achieves the optimal is given by equation (22)⁹. When densities lower than this maximum are considered, the network is spatially not

⁹A closed-form solution is unknown for this equation but standard numerical methods solve it. In our case, we use FindRoot from Wolfram Mathematica 8.

saturated and the spatial capacity of the network is still not in its highest value. In this situation, any increase of λ leads to an increase of \mathcal{C}_{IAN} until such an inflexion point is achieved. After that point, on the other hand, the network spatial throughput degrades due to the proximity of the interferers, strongly reducing the average of the link rates R^* . Consequently, \mathcal{C}_{IAN} becomes a decreasing function of λ .

From Fig. 2, we can also evaluate the proposed upper and lower bounds of the spatial capacity. As one can notice the lower bound proposed in Property 3 is loose, regardless of λ . In fact, the main use for this bound is to prove the relation between the spatial capacity and the maximum spatial throughput achieved with fixed rates, as discussed later on. Regarding the upper bound introduced in Property 4, when λ increases, the upper bound become tighter and tighter, as predict by Property 5. In other words, the upper bound has the same value as the spatial capacity \mathcal{C}_{IAN} when $\lambda \rightarrow \infty$ as shown in Fig. 2.

In the next section, we apply the same approach used here to derive the approximate spatial capacity and its properties when OPT decoders are considered.

V. OPTIMAL DECODING RULE

As previously discussed, the optimal decoding strategy when Gaussian point-to-point codes are used in wireless networks with multiple transmitter-receiver pairs consists in jointly decoding some few messages from the strongest interferers, while the rest is treated as noise. Based on this result, we obtain the achievable rates for links whose receivers use OPT decoders as follows.

Corollary 2 (achievable rates for OPT decoding rule): Assuming that the noise is Gaussian and considering that TXs use Gaussian point-to-point codes as described in Section II, then the rate R_k associated with a given link $\text{TX}_k\text{-RX}_k$ is said to be achievable when the OPT decoder is employed if, and only if, the following inequality holds:

$$R_k \leq \log_2 \left(1 + \frac{\sum_{i \in \mathcal{A}_k^*} P_{ki}}{1 + \sum_{j \in \bar{\mathcal{A}}_k^*} P_{kj}} \right) - \sum_{i \in \mathcal{A}_k^* \setminus \{k\}} R_i, \quad (37)$$

where \mathcal{A}_k^* represents the subset of transmitters whose messages are decoded by receiver k and $\mathcal{A}_k^* \cup \bar{\mathcal{A}}_k^* = \mathcal{A}$ is the set of all active transmitters in the network.

Proof: To obtain (37) we proceed with a simple manipulation of equation (3), isolating the rate R_k related to $\text{TX}_k\text{-RX}_k$ link by considering the subsets \mathcal{A}_k^* that lead to achievable rates. ■

As in Section IV, we apply the theorem stated above to statistically characterize the achievable rates over different spatial realizations using now the OPT decoding rule and then assess the average spatial capacity of the network described in Section III, which is given by equation (7). For the scenario used

throughout this section, however, the analysis is more complex since the receiver node should choose the subset of messages that will be jointly decoded and then verify whether the coding rate of its own transmitter is achievable, given all other coding rates. By construction, all receivers proceed in the same way and hence the analysis becomes a very intricate combinatorial problem. For this reason, in order to derive the pdf of the achievable rates for the OPT decoders, we resort to some approximations that will be justified afterwards.

As before, we only consider the deterministic path-loss (refer to Section IV) and that the sum of the interfering signals observed by RX_k that are treated as noise can be approximated by the signal from the closest interferer amongst them, whose power is denoted $P_{k,\text{clo}}$. If the noise power is negligible compared to $P_{k,\text{clo}}$, then $1 + \sum_{j \in \bar{\mathcal{A}}_k} P_{kj} \approx P_{k,\text{clo}}$. Based on these assumptions, we can state the following proposition.

Proposition 2 (approximate pdf of the spatial-capacity-achievable rates for OPT): Let us denote the rate tuple that achieves the spatial capacity for the network described in Section III as $\mathbf{R}^* = (R_0^*, R_1^*, \dots) \in \mathcal{R}$. Then, the pdf of R_k^* , $\forall k \in \mathcal{A}$ follows the pdf of a typical rate R^* , denoted by $f_{R^*}(x)$ and approximated as

$$f_{R^*}(x) \approx \sum_{i=0}^{\infty} \frac{(\lambda \pi d^2)^i}{\Gamma(i)} e^{-\lambda \pi d^2} f_{R^*|n}(x|n=i) \quad (38)$$

where $f_{R^*|n}(x|n)$ is the pdf of R^* given that $1+n$ messages are jointly decoded and is approximated by

$$f_{R^*|n}(x|n) \approx \ln 4 \frac{2^{(1+n)x} \lambda \pi d^2}{\alpha} \left(\frac{2^{(1+n)x} - 1}{1+n} \right)^{\frac{2}{\alpha}-1} e^{-\lambda \pi d^2 \left(\left(\frac{2^{(1+n)x} - 1}{1+n} \right)^{\frac{2}{\alpha}-1} \right)}, \quad (39)$$

such that $x > \frac{\log(2+n)}{1+n}$.

Proof: Let us first deal with the typical link TX_0 – RX_0 . Without loss of generality, we place the origin of the Cartesian plane at RX_0 and assume that all nodes that are closer to RX_0 than TX_0 have their messages jointly decoded with TX_0 message (see Fig. 3). From the distance-dependent path-loss modeling, the closer the TX, the higher the power, and then this choice of the subset \mathcal{A}_0^* is justified.

For each network spatial realization, we consider that a number n associated with the transmitters whose messages are decoded by RX_0 is known, which yields the following inequality

$$\log \left(1 + \frac{(1+n)P_{00}}{P_{0,\text{clo}}} \right) < \log \left(1 + \frac{P_{00} + \sum_{i=1}^n P_{0i}}{P_{0,\text{clo}}} \right). \quad (40)$$

One can observe from (37) and (40) that rate tuples that satisfy $R_0 + \sum_{i=1}^n R_i < \log \left(1 + \frac{(1+n)P_{00}}{P_{0,\text{clo}}} \right)$ are always achievable.

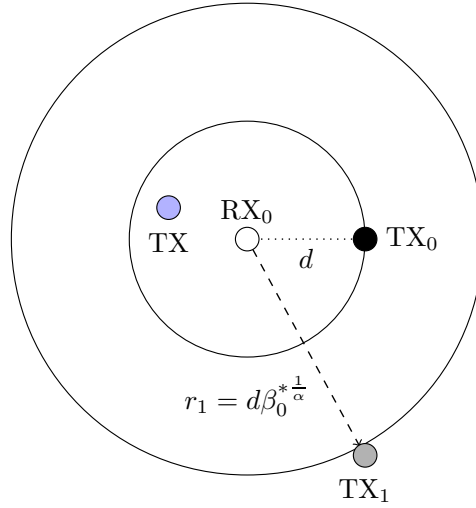


Fig. 3. Illustrative example of the typical link $\text{TX}_0\text{--RX}_0$ employing the OPT decoding rule. The blue TX has its message jointly decoded with TX_0 message and TX_1 is the closest interferer to RX_0 whose signal is treated as noise. The random variable r_1 denotes the distance between RX_0 and TX_1 such that $r_1 > d$.

Defining $\beta_0^* = P_{00}/P_{0,\text{clo}}$, we use similar steps to the ones used in the proof of Proposition 2, but considering now that $r_1 > d$ to compute the pdf $f_{\beta_0^*}(x)$ as

$$f_{\beta_0^*}(x) = \frac{2\lambda\pi d^2 x^{\frac{2}{\alpha}}}{\alpha x} e^{-\lambda\pi d^2 (x^{\frac{2}{\alpha}} - 1)}, \quad (41)$$

where $x > 1$ and $f_{\beta_0^*}(x) = 0$ when $x \leq 1$.

Then, we assume that $R_0 + \sum_{i=1}^n R_i \approx (1+n)R_0$ to obtain $(1+n)R_0^* = \log(1 + (1+n)\beta_0^*)$. By applying such a transformation, we can find the pdf of R_0^* given n . Here we use the proprieties of Palm distributions in PPPs (refer to the proof of Proposition 2) and then the index 0 can be dropped, resulting in equation (39). To unconditioned the pdf $f_{R^*|n}(x|n)$, we apply the definition of Poisson process to compute the probability that $n = i$ points lie in the area πd^2 , concluding this proof. ■

Remark: In addition to the closest interferer treated as noise approximation, this proposition is based on other two main assumptions: (i) the detected power at RX_0 related to the $1+n$ jointly decoded messages is equal to $(1+n)P_{00}$ and (ii) the sum rate associated with those messages is given by $(1+n)R_0$. In assumption (i), we use the lower bound given by (40), which indicates that we underestimate the aggregate power, while in (ii) we approximate the sum of $1+n$ random variables that follows the same distribution by one random variable multiplied by $1+n$. We argue that the underestimation byproduct of assumption (i) leaves us some room for variations in the sum rate approximation used in (ii). In addition, due to the homogeneity of the spatial process, $R_0 + \sum_{i=1}^n R_i \approx (1+n)R_0$ leads to a reasonable approximation. Simulations results are presented in Section VII where we discuss such approximations.

Here we can compute the approximate average spatial capacity¹⁰ \mathcal{C}_{OPT} when the OPT decoding rule is employed as

$$\mathcal{C}_{\text{OPT}} \approx \lambda \int_0^\infty x f_{R^*}(x) dx, \quad (42)$$

where $f_{R^*}(x)$ is given in Proposition 2.

The integral in (42) is analytically unsolvable (we can rely on numerical solutions, though). To gain more insights on the system performance, we next derive some properties of the spatial capacity.

Property 6 (concavity): Considering that the rate R^* is a function of the network density λ , then \mathcal{C}_{OPT} given by (42) is *quasi concave* in terms of λ , where R^* is a random variable given by (38).

Property 7 (lower bound): A lower bound of the spatial capacity given by (42) is computed as

$$\mathcal{C}_{\text{OPT}} \geq \lambda \sum_{i=0}^{\infty} \frac{(\lambda \pi d^2)^i}{\Gamma(i)} y e^{-\lambda \pi d^2} \left(\frac{2^{(1+i)y-1}}{1+i} \right)^{\frac{2}{\alpha}}, \quad (43)$$

where $y > \frac{\log_2(2+i)}{1+i}$ for all $i \geq 0$.

Property 8 (upper bound): A upper bound of the spatial capacity given by (42) is computed as

$$\mathcal{C}_{\text{OPT}} \leq \lambda \sum_{i=0}^{\infty} \frac{(\lambda \pi d^2)^i}{\Gamma(i)} \frac{e^{-\lambda \pi d^2}}{1+i} \log_2 \left(1 + (1+i) \left(\frac{1}{\lambda \pi d^2} \right)^{\frac{2}{\alpha}} \Gamma \left(1 + \frac{2}{\alpha}, \lambda \pi d^2 \right) e^{\lambda \pi d^2} \right), \quad (44)$$

where $\Gamma(\cdot, \cdot)$ is the incomplete Gamma function, which is defined as $\Gamma(z, a) = \int_a^\infty t^{z-1} e^{-t} dt$.

Property 9 (asymptotic equivalence): Let \sim denote asymptotic equivalence of two functions, then

$$\mathcal{C}_{\text{OPT}} \sim \lambda \sum_{i=0}^{\infty} \frac{(\lambda \pi d^2)^i}{\Gamma(i)} \frac{e^{-\lambda \pi d^2}}{1+i} \log_2 \left(1 + (1+i) \left(\frac{1}{\lambda \pi d^2} \right)^{\frac{2}{\alpha}} \Gamma \left(1 + \frac{2}{\alpha}, \lambda \pi d^2 \right) e^{\lambda \pi d^2} \right), \quad (45)$$

when $\lambda \rightarrow \infty$.

The proofs of these properties follow the same principles used in the previous section so we do not present them here. It is worth pointing though out that the proofs of (43)-(45) begin by assuming that the number $1+n$ of jointly decoded messages is known. Then, we use the fact that the unconditioned spatial capacity is a linear combination of the conditioned capacities with weights given by the Poisson probabilities that $n=i$ nodes lie in a area of πd^2 , resulting in the probability $\frac{(\lambda \pi d^2)^i}{\Gamma(i)} e^{-\lambda \pi d^2}$.

Next, we present a proposition that states that the OPT decoding rule always leads to a better performance than the IAN rule.

¹⁰As in the previous section we use the term spatial capacity to refer to the approximate average spatial capacity.

Proposition 3 (\mathcal{C}_{OPT} vs. \mathcal{C}_{IAN}): For any given network density λ ,

$$\mathcal{C}_{\text{OPT}} \geq \mathcal{C}_{\text{IAN}}. \quad (46)$$

Proof: To prove this proposition, we first use the identity $a \log_2(1+x) \leq \log_2(1+ax) \forall a \geq 1$ to verify that

$$\int_1^\infty x^{\frac{2}{\alpha}-1} \frac{\log_2(1+(1+n)x)}{1+n} e^{-\lambda\pi d^2 x^{\frac{2}{\alpha}}} dx \geq \int_0^\infty x^{\frac{2}{\alpha}-1} \log_2(1+x) e^{-\lambda\pi d^2 (x^{\frac{2}{\alpha}}-1)} dx, \quad (47)$$

where $n \in \mathbb{N}$ represents the number of jointly decoded messages by the typical link $\text{TX}_0\text{-RX}_0$.

Recalling that all TXs that are located closer to RX_0 than TX_0 have their messages jointly decoded by RX_0 , then the number n follows a Poisson distribution over an area of πd^2 . Using this fact and multiplying both sides of (47) by $\frac{2\lambda\pi d^2}{\alpha}$, we have the following inequality:

$$\sum_{i=0}^\infty \frac{(\lambda\pi d^2)^i}{\Gamma(i)} e^{-\lambda\pi d^2} \int_1^\infty f_{\beta^*}^{\text{OPT}}(x) \frac{\log_2(1+(1+i)x)}{1+i} dx \geq \sum_{i=0}^\infty \frac{(\lambda\pi d^2)^i}{\Gamma(i)} e^{-\lambda\pi d^2} \int_0^\infty f_{\beta^*}^{\text{IAN}}(x) \log_2(1+x) dx, \quad (48)$$

where $f_{\beta^*}^{\text{OPT}}(x)$ and $f_{\beta^*}^{\text{IAN}}(x)$ are given by (41) and (16), respectively.

To conclude this proof, we multiply both sides of (48) by λ , obtaining then (46). ■

In Fig. 4, we present the spatial capacity \mathcal{C}_{OPT} given by (42) as a function of λ together with its proposed upper and lower bounds. One can observe that the lower bound given by Property 7 is very loose for the value of the constant y that was arbitrarily chosen ($y = 2$). This bound, however, can be improved by tuning the constant y in accordance to the number of jointly decoded messages. Such an improvement in the proposed bound will be discussed in the next section when we apply it to analytically assess the performance of networks where predetermined fixed rates are imposed.

Turning your attention to the values of \mathcal{C}_{OPT} given by (42), one can easily see that it is an increasing function of λ . For lower densities, \mathcal{C}_{OPT} increases faster since the probability that an interfering TX has its message jointly decoded is also low and, consequently, the rate is constrained by the interferers that are treated as noise, indicating that \mathcal{C}_{OPT} is limited by the low spatial reuse. When λ increases, on the other hand, more messages from interfering TXs start being jointly decoded, which diminishes the \mathcal{C}_{OPT} rate of increase. Furthermore, we can observe that the upper bound proposed in Property 8 is a good approximation to \mathcal{C}_{OPT} for all densities λ especially when $\lambda \rightarrow \infty$, corroborating Property 9.

By comparing the results shown in Fig. 2 (IAN) and Fig. 4 (OPT), one can see that the OPT decoding rule provides higher spatial capacities, regardless of the network density, as predicted by Proposition 3.

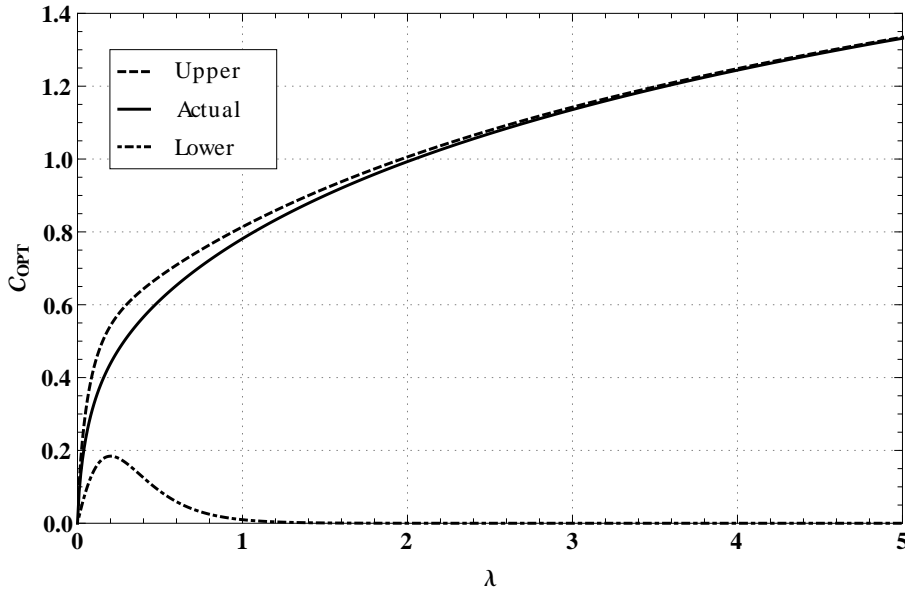


Fig. 4. Actual values, lower and upper bounds of the spatial capacity, C_{OPT} , versus the network density λ for $\alpha = 4$ and $d = 1$. The lower bound is obtained using $\gamma = 2$ in equation (43). The actual values and upper bound are computed using equations (42) and (44), respectively.

The performance gain obtained with the OPT decoder in comparison with the IAN decoder indicates that the mechanism of joint detection used here is a good way to deal with the strongest interferers. A more detailed comparative analysis between OPT and IAN decoding rules is presented later.

In the following section, we compare the results obtained so far with the most usual approach found in the literature (e.g. [12]): coding rates are fixed for a given network density and set to optimize the average spatial throughput regardless of a specific network topology, leading to outage events (i.e. some pairs use coding rates above their channel capacity).

VI. SPATIAL THROUGHPUT OPTIMIZATION USING PREDETERMINED FIXED RATES

We now focus our attention on scenarios where TXs set their coding rates to the fixed values that leads to the highest average spatial throughput, given that the TXs are aware of how many messages are jointly decoded by their RXs. Using this scheme, groups of TXs use the same fixed coding rates and then an optimization problem is formulated to find these rates such that the average spatial throughput is maximized. As a consequence the optimal choice of coding rates, as discussed later on, is not in the network capacity region, stated in Theorem 1, leading to outage events for some links. Next, we present the definition of the aforementioned optimization problem.

Definition 5 (highest spatial throughput): The spatial throughput optimization problem for a network where TXs have fixed coding rates is defined as

$$\mathcal{T} = \max_{\mathbf{R}} \mathbb{E}[\mathcal{S}], \quad (49)$$

where \mathcal{T} is the maximum spatial throughput, $\mathbf{R} = (R_0, R_1, \dots)$ represents the set of fixed coding rates R_i used by the TXs such that i is the number of jointly decoded messages in addition to the desired one, and \mathcal{S} is the spatial throughput given by (5), where only the successful transmissions are taking into account.

When the IAN decoding rule is used, there is no jointly decoded message and then the optimization is only related to one fixed coding rate¹¹. We now present two propositions that state the highest spatial throughputs for IAN and OPT decoders applying the network modeling used before¹².

Proposition 4 (highest spatial throughput for IAN): The highest spatial throughput \mathcal{T}_{IAN} achieved when IAN decoders are used is given by

$$\mathcal{T}_{\text{IAN}} = \lambda \log_2(1 + \beta^*) e^{-\lambda \pi d^2 \beta^{*\frac{2}{\alpha}}}, \quad (50)$$

where β^* is the value of $\beta > 0$, which is solution of

$$\beta = \left(\frac{2}{\alpha} \lambda \pi d^2 (1 + \beta) \ln(1 + \beta) \right)^{\frac{\alpha}{\alpha-2}}. \quad (51)$$

Proof: Let us first write the spatial throughput given by (5) for this scenario as

$$\mathcal{S} = \lambda R P_s, \quad (52)$$

where R is the fixed coding rate used by all TXs and P_s is the success probability associated with R .

We proceed here similarly to the proof of Proposition 1 and then apply the relation $R = \log_2(1 + \beta)$, where $R, \beta > 0$. From the dominant interferer assumption, an outage event occurs whenever an interfering TX node lies inside the area defined by the circumference centered at the RX node and with radius $d\beta^{\frac{1}{\alpha}}$. Using the Poisson distribution, we have that $P_s = e^{-\lambda \pi d^2 \beta^{\frac{2}{\alpha}}}$. Hence, we can rewrite equation (52) as

$$\mathcal{S} = \lambda \log_2(1 + \beta) e^{-\lambda \pi d^2 \beta^{\frac{2}{\alpha}}}, \quad (53)$$

which is a concave function of β .

Hence, we compute β^* which is the solution of the derivative equation $d\mathcal{S}/d\beta = 0$, resulting after some manipulation in (51). To conclude this proof, we use β^* into equation (53), obtaining (50). ■

Proposition 5 (highest spatial throughput for OPT): The highest spatial throughput \mathcal{T}_{OPT} achieved when OPT decoders are used is given by

$$\mathcal{T}_{\text{OPT}} = \lambda \sum_{i=0}^{\infty} \frac{(\lambda \pi d^2)^i}{\Gamma(i)} \frac{e^{-\lambda \pi d^2}}{1+i} \log_2(1 + (1+i)\beta_i^*) e^{-\lambda \pi d^2 \left(\beta_i^{*\frac{2}{\alpha}} - 1 \right)} \quad (54)$$

where, for each $i = 0, 1, 2, \dots$, β_i^* is found as the value of $\beta_i > 1$, which is solution of

¹¹This is the usual approach as in [12], [24].

¹²Once again we use the closest intereferer treated as noise approximation. Besides, the term highest spatial throughput refers to the highest approximate spatial throughput.

$$\beta_i = \left(\frac{2}{(1+i)\alpha} \lambda \pi d^2 (1 + (1+i)\beta_i) \ln(1 + (1+i)\beta_i) \right)^{\frac{\alpha}{\alpha-2}}. \quad (55)$$

Outline of proof: To prove this proposition, we follow the same steps used in the proof of Proposition 4, considering these basic differences: $\beta_i = d^{-\alpha}/r_1^{-\alpha} > 1$ (since messages from TXs closer to a given RX than its own TX are jointly decoded and then $r_1 > d$) and the optimization is proceeded for each $i = 0, 1, 2, \dots$ which yields (55). To conclude this outline, we average the spatial throughputs by the Poisson probabilities that i nodes lie in the area πd^2 , resulting in (54). ■

Here we apply Properties 3 and 7 to obtain an analytical relation between the spatial capacity \mathcal{C} and the highest spatial throughput \mathcal{T} using fixed rates for either decoding rules.

Proposition 6 (\mathcal{C} vs. \mathcal{T}): For a given density λ and assuming that all links use the same decoding rule (either IAN or OPT), then

$$\mathcal{C} \geq \mathcal{T}. \quad (56)$$

Proof: This statement is a consequence of Property 3, when we set the constant $y = \log(1 + \beta^*)$ in (24), yielding (50). Similarly, we use Property 7, applying for each different $i \in \mathbb{N}$ a different constant y in (43) such that $y_i = \frac{\log(1+(1+i)\beta_i^*)}{1+i}$, which yields (54), concluding this proof. ■

Fig. 5 shows the maximum spatial throughput following the formulation derived in this section. As proved in Proposition 6, \mathcal{T} is always lower than or equal to \mathcal{C} for the same density and the same decoding rule. This is justified by the methodology used to derive the spatial capacity, which allows for a coding rate setting based on the relative positions of the nodes for each different realization of the spatial process. When fixed rates are used, the transmitters code their messages using a fixed rate that depends only on the number of other messages that are jointly decoded by their own receivers. By optimizing based only on the average behavior of the network, some RXs cannot successfully decode their messages for specific topologies, which decreases the spatial throughput. Therefore, the spatial-capacity-achieving strategy has always a better performance. Besides given the decoding rule employed, the curves of \mathcal{T} and \mathcal{C} have a similar shape.

Fig. 5 also shows that the spatial capacity obtained when OPT is used has a huge gain if compared with the IAN option. As predicted by Proposition 3, this result reflects that the OPT rule is able to avoid the strongest interferers by jointly decoding their messages. When the density λ is low, both OPT and IAN decoders have approximately the same performance since the probability that a interferer is closer to a given RX than its own TX is very low. Increasing λ , such a probability also increases and then the

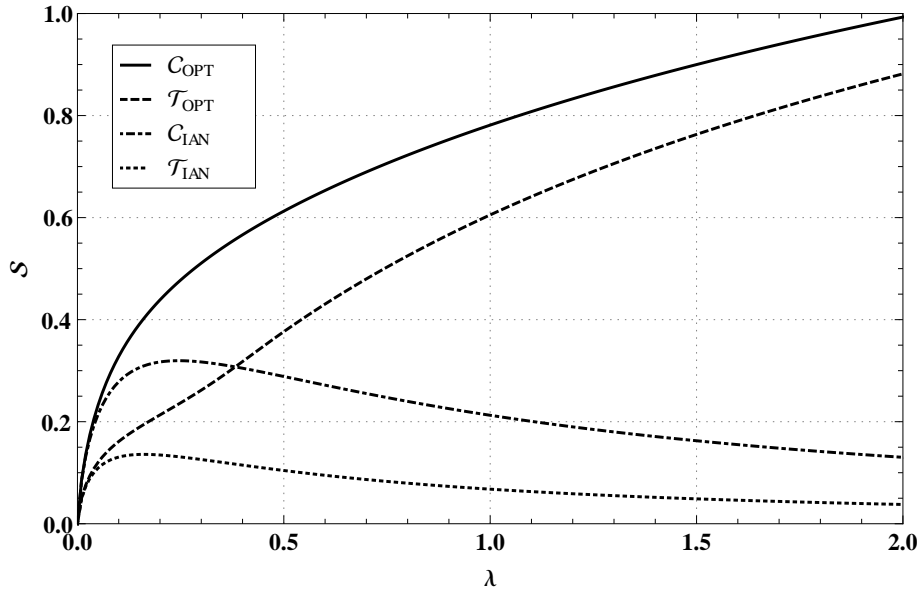


Fig. 5. The highest spatial throughputs \mathcal{T} using fixed coding rates given by (50) and (54), and the spatial capacities \mathcal{C} given by (17) and (42) as a function of the network density λ for IAN and OPT decoding rules, $d = 1$ and $\alpha = 4$.

differences between the strategies become apparent as the closest interferer is the limiting factor for IAN, while such node may have its message jointly decoded when OPT is used, what decreases the harmful effects of the nearby interferers.

VII. DISCUSSIONS

So far we have showed that, for same network density, (i) OPT decoders outperform IAN, and (ii) the spatial-capacity-achieving strategy outperforms the average spatial throughput optimization when receivers employ the same decoding rule. Nevertheless we still need to discuss some possible limitations of our finds, namely the tightness of our approximations and the feasibility of each decoding rule for practical implementations. In the following subsections we deal with both aspects, identifying why our results are important even when our approximation is poor and for which circumstances the design setting that provides the worst performance is more suitable than the optimal.

A. Tightness of our approximation

Here we discuss the validity of the “closest interferer treated as noise approximation” used to derive the approximate performance of both decoding rules. Figure 6 shows the average spatial capacity \mathcal{C} computed using our analytical approximation and Monte Carlo simulation as a function of the network density λ for both decoders¹³. For both IAN and OPT, the lower the density is, the better our approximation works.

¹³The results for the highest average spatial throughput presented in Section VI follows the same trends and thus we exclude them from the paper.

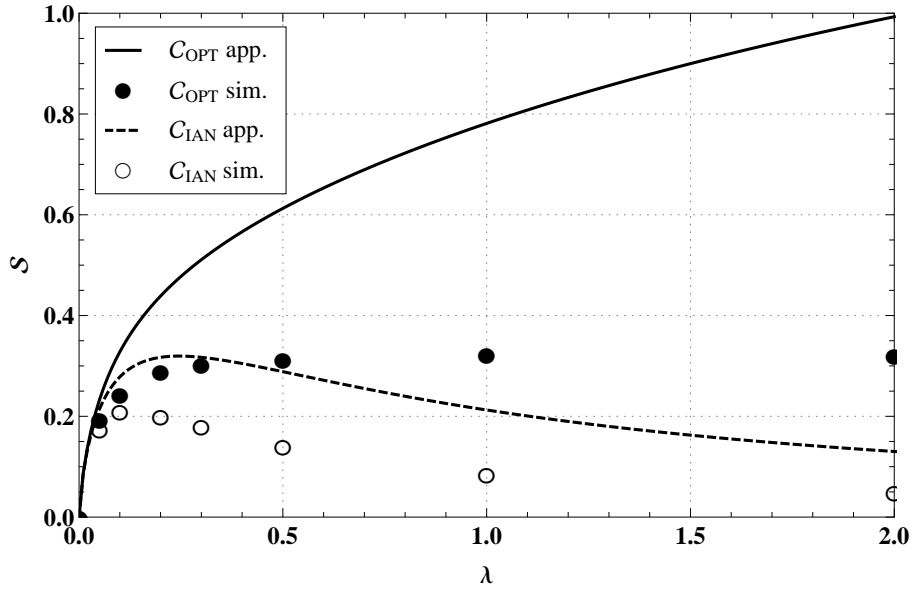


Fig. 6. Spatial capacities C for IAN and OPT as a function of the network density λ , $d = 1$ and $\alpha = 4$. Approximate results given by equations (17) and (42), and simulations.

Conversely, increasing the density, our approximate spatial capacity gets looser and looser.

The closest interferer approximation is in fact a lower bound of the aggregate interference [12], leading then to an upper bound of the actual spatial capacity. This bound have been proved to be asymptotically equivalent to the actual values when $\lambda \rightarrow 0$ [12], [25]¹⁴. For higher densities, the closest interferer treated as noise tends to contribute less to the aggregate interference experienced by the receivers, worsening our approximation. Besides, we obtained our numerical results using the path-loss exponent $\alpha = 4$ and Weber et al. showed that lower exponents lead to looser bounds [9].

Yet, the comparison between the IAN and OPT decoders is fair since the results presented in Sections IV and V rely on the same approximation¹⁵. We further argue that our approximation has no effect in the trade-off analysis done in this paper and Figure 6 illustrates this fact by showing that the OPT always outperforms IAN in similar scales: the ratios $C_{\text{IAN}}/C_{\text{OPT}}$ obtained via simulation or via our approximations have similar values when considering the same λ . As the proposed formulation provides a much simpler way to assess the network performance than numerical simulations, we reinforce the contribution of this paper even when our approximations provide poor bounds.

All in all, we believe that our main messages – OPT is better than IAN, and spatial-capacity achieving strategy is better than the best fixed rate one – are unaffected by our approximations. Despite of these facts,

¹⁴In our point of view this asymptotic analysis is unsuitable for the study carried out here; we assume an interference-limited network, which opposes the idea of very low density of interferers. When $\lambda \rightarrow 0$, we see the network in its noise-limited regime.

¹⁵We can argue in the same way to say that the analysis presented in Section VI is also fair.

the optimal strategy is many times unfeasible for practical implementation as discussed in the following.

B. Design setting and mobility pattern

Throughout this paper we have shown that the best design option in terms of spatial throughput is to employ OPT decoders and apply the spatial-capacity achieving scheme. This solution, however, has drawbacks: (i) RXs require the knowledge of the codebooks of the jointly decoded messages and (ii) OPT decoders are computationally more complex than IAN.

Knowing them, we argue that the use of either/both OPT and/or spatial-capacity achieving strategy is unfeasible for (highly) mobile topologies. Under this topology, the neighbors of any given receiver vary very fast, making impossible the joint decoding procedure. Shopping malls and streets where people frequently come and go can exemplify this scenario. If this is the case, even though the design setting employing IAN decoders with fixed rate optimization is far from the optimal performance, it is a more suitable choice.

Conversely, when (quasi-)static networks are considered, the optimal strategy becomes possible. In this case, receiver nodes must know the codebooks of their strongest interfering nodes and jointly decode their messages. In addition, the links must coordinate their coding rates to be in the network capacity region. Smart homes, industry plants and other kind of machine-to-machine communications can exemplify this mobility pattern.

Besides, there are other aspects that may be prohibitive for OPT. For instance, many applications require secrecy and then the codebook knowledge makes OPT unfeasible even for static topologies. Other applications need fast processing time, which is also unfeasible when many interfering messages are jointly decoded. Anyway, this dependence of the topology must be taken into account when the network is designed. Furthermore, the mobility pattern of the network can also change over time – for example, offices during the night are quasi-static, while highly dynamic during parts of the working hours. All these aspects indicate the needs for adaptive algorithms that may assess the network state and proceed with their optimization accordingly.

VIII. FINAL REMARKS

In this paper we studied the spatial throughput of interference networks using Gaussian point-to-point codes. More specifically we evaluated two different decoding rules: (i) treating all interfering messages as noise – IAN, and jointly decoding the messages whose detected power is higher than the desired message power while treating the others as noise – OPT.

We proposed an approximation of the highest spatial throughput for Poisson distributed networks such that all links work in their capacity region (spatial-capacity achieving strategy). We then stated several properties of our approximation using either decoders and prove that, when the same network density is assumed, (i) the OPT always outperforms IAN, and (ii) the spatial-capacity-achieving strategy is always better than the predetermined fixed rate optimization, where transmitters code their messages in order to optimize the average spatial throughput.

REFERENCES

- [1] V. Chandrasekhar, J. Andrews, and A. Gatherer, "Femtocell networks: A survey," *IEEE Commun. Mag.*, vol. 46, no. 9, pp. 59–67, Sep. 2008.
- [2] J. Andrews, S. Shakkottai, R. Heath, N. Jindal, M. Haenggi, R. Berry, D. Guo, M. Neely, S. Weber, S. Jafar, and A. Yener, "Rethinking information theory for mobile ad hoc networks," *IEEE Commun. Mag.*, vol. 46, no. 12, pp. 94–101, Dec. 2008.
- [3] A. Carleial, "Interference channels," *IEEE Trans. Inf. Theory*, vol. 24, no. 1, pp. 60–70, Jan. 1978.
- [4] A. Gamal and Y. Kim, *Network Information Theory*. Cambridge University Press, 2012.
- [5] P. Gupta and P. Kumar, "The capacity of wireless networks," *IEEE Trans. Inf. Theory*, vol. 46, no. 2, pp. 388–404, Mar. 2000.
- [6] F. Xue and P. Kumar, "Scaling laws for ad hoc wireless networks: An information theoretic approach," *NOW*, vol. 1, no. 2, pp. 145–270, 2006.
- [7] M. Franceschetti, M. D. Migliore, and P. Minero, "The capacity of wireless networks: Information-theoretic and physical limits," *IEEE Trans. Inf. Theory*, vol. 55, no. 8, pp. 3413–3424, Aug. 2009.
- [8] M. Franceschetti, M. D. Migliore, P. Minero, and F. Schettino, "The degrees of freedom of wireless networks via cut-set integrals," *IEEE Trans. Inf. Theory*, vol. 57, no. 5, pp. 3067–3079, May 2011.
- [9] S. Weber, X. Yang, J. Andrews, and G. de Veciana, "Transmission capacity of wireless ad hoc networks with outage constraints," *IEEE Trans. Inf. Theory*, vol. 51, no. 12, pp. 4091–4102, Dec. 2005.
- [10] M.-S. Alouini and A. Goldsmith, "Area spectral efficiency of cellular mobile radio systems," *IEEE Trans. Veh. Technol.*, vol. 48, no. 4, pp. 1047–1066, Jul. 1999.
- [11] A. Baddeley, "Spatial point processes and their applications," in *Stochastic Geometry*. Springer, 2007, pp. 1–75.
- [12] S. Weber and J. Andrews, "Transmission capacity of wireless networks," *NOW*, vol. 5, no. 2-3, pp. 109–281, 2012.
- [13] R. Vaze, "Throughput-delay-reliability trade-off with ARQ in wireless ad hoc networks," *IEEE Trans. Wireless Commun.*, vol. 10, no. 7, pp. 2142–2149, Jul. 2011.
- [14] P. H. J. Nardelli, P. Cardieri, and M. Latva-aho, "Efficiency of wireless networks under different hopping strategies," *IEEE Trans. Wireless Commun.*, vol. 11, no. 1, pp. 15–20, Jan. 2012.
- [15] —, "Maximising transmission capacity of ad hoc networks via transmission system design," *Electron. Lett.*, vol. 47, no. 5, pp. 348–349, Mar. 2011.
- [16] P. H. J. Nardelli, M. Kaynia, P. Cardieri, and M. Latva-aho, "Optimal transmission capacity of ad hoc networks with packet retransmissions," *IEEE Trans. Wireless Commun.*, vol. 11, no. 8, pp. 2760–2766, Aug. 2012.
- [17] R. K. Ganti, J. Andrews, and M. Haenggi, "High-SIR transmission capacity of wireless networks with general fading and node distribution," *IEEE Trans. Inf. Theory*, vol. 57, no. 5, pp. 3100–3116, 2011.
- [18] H. Takagi and L. Kleinrock, "Optimal transmission ranges for randomly distributed packet radio terminals," *IEEE Trans. Commun.*, vol. 32, no. 3, pp. 246–257, Mar. 1984.

- [19] F. Baccelli and B. Blaszczyszyn, “Stochastic geometry and wireless networks: Theory,” *NOW*, vol. 3, no. 3-4, pp. 249–449, 2009.
- [20] —, “Stochastic geometry and wireless networks: Applications,” *NOW*, vol. 4, no. 1-2, pp. 1–312, 2009.
- [21] M. Haenggi, J. Andrews, F. Baccelli, O. Dousse, and M. Franceschetti, “Stochastic geometry and random graphs for the analysis and design of wireless networks,” *IEEE J. Sel. Areas Commun.*, vol. 27, no. 7, pp. 1029–1046, Sep. 2009.
- [22] P. Cardieri, “Modeling interference in wireless ad hoc networks,” *Commun. Surveys Tuts.*, vol. 12, no. 4, pp. 551–572, May 2010.
- [23] F. Baccelli, A. El Gamal, and D. Tse, “Interference networks with point-to-point codes,” *IEEE Trans. Inf. Theory*, vol. 57, no. 5, pp. 2582–2596, May 2011.
- [24] J. Blomer and N. Jindal, “Transmission capacity of wireless ad hoc networks: successive interference cancellation vs. joint detection,” in *Proc. of 2009 IEEE International Conference on Communications*.
- [25] V. Mordachev and S. Loyka, “On node density - outage probability tradeoff in wireless networks,” *IEEE J. Sel. Areas Commun.*, vol. 27, no. 7, pp. 1120–1131, Sep. 2009.
- [26] R. Vaze and R. Heath, “Transmission capacity of ad-hoc networks with multiple antennas using transmit stream adaptation and interference cancellation,” *IEEE Trans. Inf. Theory*, vol. 58, no. 2, pp. 780–792, Feb. 2012.
- [27] K. Huang, J. Andrews, D. Guo, R. Heath, and R. Berry, “Spatial interference cancellation for multi-antenna mobile ad hoc networks,” *IEEE Trans. Inf. Theory*, vol. 58, no. 3, pp. 1660–1676, Mar. 2012.
- [28] V. Cadambe and S. Jafar, “Interference alignment and degrees of freedom of the K -user interference channel,” *IEEE Trans. Inf. Theory*, vol. 54, no. 8, pp. 3425–3441, Aug. 2008.
- [29] M. Yacoub, *Foundations of mobile radio engineering*. CRC Press, 1993.
- [30] H. Inaltekin, M. Chiang, H. Poor, and S. Wicker, “On unbounded path-loss models: effects of singularity on wireless network performance,” *IEEE J. Sel. Areas Commun.*, vol. 27, no. 7, pp. 1078–1092, Sep. 2009.
- [31] M. Haenggi, “On distances in uniformly random networks,” *IEEE Trans. Inf. Theory*, vol. 51, no. 10, pp. 3584–3586, Oct. 2005.